Electron. Mater. Lett., Vol. 10, No. 1 (2014), pp. 67-72
DOI: 10.1007/s13391-013-3077-3

Correlation between Luminescence and Defects in Nonpolar and Semipolar InGaN/GaN Quantum Wells on Planar and Patterned Sapphire Substrates

Seunga Lee, Geunho Yoo, Jongjin Jang, Youngjong Won, and Okhyun Nam*

LED Technology Center, Department of Nano-Optical Engineering, Korea Polytechnic University, Siheung 429-839, Korea

(received date: 25 March 2013 / accepted date: 19 June 2013 / published date: 10 January 2014)

The optical and structural properties of nonpolar and semipolar InGaN/GaN quantum wells (QWs) grown on planar sapphire substrates and patterned sapphire substrates (PSSs) were investigated in order to understand the effect of defects on the luminescence. By introducing the PSS technique, surface morphological features were varied in number and size, and the defect density was significantly reduced by the PSS patterns, which resulted in the formation of low-defect regions. The photoluminescence (PL) analyses of nonpolar and semipolar QWs samples revealed that the semipolar ($11\bar{2}2$) QWs, which had better optical performance and higher In incorporation, are more suitable for application to long-wavelength emitters in the green-red spectral range and beyond. Moreover, particularly in the semipolar QWs, we could observe that the optical properties were enhanced by the decrease in defect density. It was also noted that In incorporation was increased in the high-defect regions and in the regions where arrowhead-like features existed.

Keywords: III-nitride semiconductor, nonpolar/semipolar quantum wells, defects, luminescence

1. INTRODUCTION

In recent years, Group III nitrides have been intensely investigated owing to their significant potential in a variety of applications, ranging from high-efficiency solid-state lighting and photovoltaics to high-power and high-temperature electronics.[1-3] $In_xGa_{1-x}N$ alloys, in particular, are of great interest for solid-state lighting and photovoltaics in that the bandgap of these materials can be tuned from the near-ultraviolet region to the near-infrared region by changing the In composition.[4,5] However, because there remains considerable difficulty in making high-quality InGaN films, many researchers have attempted to synthesize InGaN layers with tunability across the entire range of compositions. In the case of InGaN-based optoelectronic devices such as light-emitting diodes and laser diodes, one approach is to grow InGaN layers on nonpolar or semipolar planes. This is an effective way to remove or reduce the polarization-related electric fields that cause a reduction in radiative recombination efficiency and a blueshift in the peak emission wavelength with increasing carrier density observed in conventional *c*-plane emitters.[6-8] However, when the InGaN layer is grown directly on foreign substrates such as sapphire substrates, these nonpolar and semipolar films usually contain a high density of extended defects, mainly basal stacking faults (BSFs) and partial dislocations (PDs),[9,10] which are detrimental to the optical and electrical properties.[11] Thus, various techniques such as the use of patterned sapphire substrate (PSS),[12,13] epitaxial lateral overgrowth,[14] and the fabrication of nanoporous GaN by photoenhanced electrochemical etching[15] have been employed to improve the crystal quality of nonpolar and semipolar films. Although research on these techniques is necessary for applying the nonpolar and semipolar growth to device fabrication, we consider that understanding the correlation between defects and In dynamics is also important to overcome the problems of nonpolar and semipolar films. For these reasons, in this study we investigated the structural and optical properties of nonpolar ($11\bar{2}0$) and semipolar ($11\bar{2}2$) InGaN/GaN quantum wells (QWs) grown using the PSS technique.

2. EXPERIMENTAL PROCEDURE

A series of nonpolar ($11\bar{2}0$) and semipolar ($11\bar{2}2$) InGaN/GaN QWs were grown by metal-organic chemical vapour deposition using trimethylgallium, trimethylindum, and ammonia as precursors. The nonpolar films were grown on a planar *r*-plane sapphire substrate and a patterned *r*-plane sapphire substrate (*r*-PSS), and the semipolar films were grown on a planar *m*-plane sapphire substrate and a patterned *m*-plane sapphire substrate (*m*-PSS). The nonpolar samples were labelled as N1 and N2 and the semipolar samples were labelled as S1 and S2. For the *m*-PSS sample, patterns with smaller sizes and larger spacing than those in the *r*-PSS patterns were used because of the difficulty in the coalescence

*Corresponding author: ohnam@kpu.ac.kr

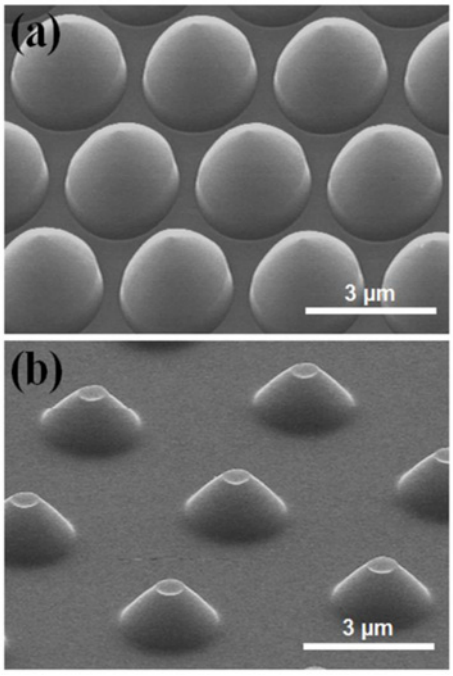

Fig. 1. SEM images of (a) *r*-PSS and (b) *m*-PSS.

of the film (the diameter, height, and interval of each pattern for the *r*-PSS sample were 2.7, 1.3, and 0.3 m, respectively, and those of each pattern for the *m*-PSS sample were 2.5, 0.7, and 2.5 μm, respectively [see Figs. 1(a) and (b)]).

On these substrates, InGaN/GaN QW structures were grown as follows: a 7-μm-thick nonpolar undoped GaN layer was grown at 1040°C and 100 Torr with a low V/III ratio of 900 first on top of the substrate (for the semipolar growth, a 6-μm-thick semipolar undoped GaN layer was grown in an H_2 atmosphere at a temperature of 1050°C to coalesce the film), followed by five periods of InGaN/GaN QW with 6-nm GaN barrier and 2.3-nm InGaN wells deposition. After that, these QW structures were capped with a 0.13-μm-thick GaN layer grown on top of the last barrier.

The structural properties were examined by optical microscopy (OM) and cross-sectional transmission electron microscopy (TEM). For the TEM analyses, the specimens were prepared by mechanical polishing, followed by ion-beam milling to electron transparency. Scanning electron microscopy (SEM) and cathodoluminescence (CL) were carried out at room temperature and 10 kV using a Hitachi S-4300SE equipped with a Gatan MonoCL3 system. In addition, micro-photoluminescence (μ-PL) was used to measure the optical properties of the QWs at room temperature. A 325 nm He-Cd laser was used as the PL excitation source. A reflecting microscope objective lens (×39) was used for μ-PL measurements to control the beam spot size and collect the signal at the same time. The resolution for the μ-PL mapping was approximately 1 μm, and the laser power was maintained at 1.8 mW.

3. RESULTS AND DISCUSSION

The surface morphology of samples N1, N2, S1, and S2 were observed by OM. In general, it is known that GaN-based films exhibit some specific features on the surface with the grown plane. For nonpolar $(11\bar{2}0)$ films grown on an *r*-plane sapphire substrate, undulating structures are commonly observed parallel to the *c*-axis,[16] whereas semipolar $(11\bar{2}2)$ films grown on an *m*-plane sapphire substrate show arrowhead-like features along the $[\bar{1}\bar{1}23]$ direction on the surface.[18] These two types of surface morphology were also observed in our samples. However, as shown in Fig. 2, it is clearly seen that the number and size of the surface features were significantly different with the type of substrates. Regardless of the growth plane, the samples grown on the planar substrates showed a high density of small features on the surfaces [see Figs. 2(a) and (c)], whereas the samples grown on the PSSs showed a low density of large features [see Figs. 2(b) and (d)]. Because the surface features were greatly modified by anisotropic in-plane strain and the adatom diffusion length,[16,17] the results for samples N2 and S2 [Figs. 2(b) and (d)] were attributed to the increase in Ga migration length owing to the reduction in defect density.

Figure 3 shows cross-sectional TEM images of nonpolar and semipolar GaN layers grown on the PSS to confirm the reduced defect density of samples N2 and S2. In both samples, we could see that each TEM image indicated two distinct regions: a low-defect region and a high-defect region. In the high-defect region, the high density of defects originated from the seed layer and propagated to the film surface, whereas the number of defects was drastically reduced by

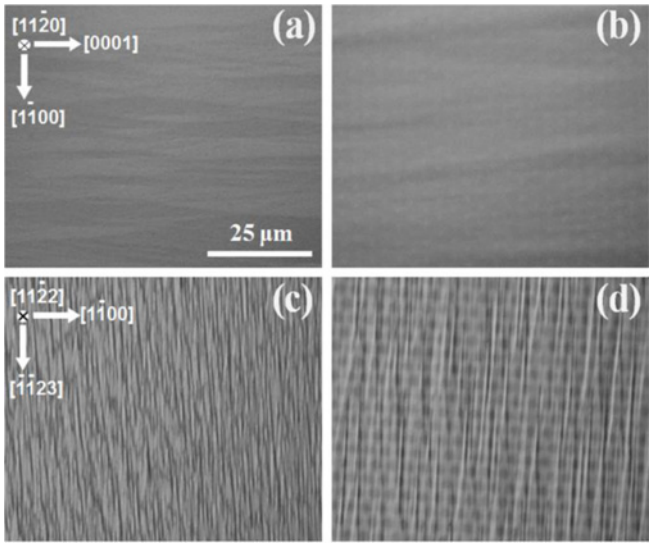

Fig. 2. Surface morphology of samples (a) N1, (b) N2, (c) S1, and (d) S2 by optical microscopy.

the PSS pattern in the low-defect region. This means that the PSS patterns had a considerable impact on the distribution of the defect density and contributed to improving the crystal quality of the samples. Other structural characteristics shown in our prior reports (not shown here) also supported these arguments. For the nonpolar GaN layers,[13] the results from the on-axis (11$\bar{2}$0) x-ray rocking curves (XRCs) measured along the parallel and vertical direction to the [0001] revealed that the full width at half maximum (FWHM) value of the nonpolar GaN layer grown on planar substrate was 770 and 2156 arcsec, respectively, and those of the nonpolar GaN layer grown on PSS was 468 and 756 arcsec, respectively. These results implied that defect densities were significantly reduced by introducing the PSS. Moreover, it was more clearly seen in the plan-view TEM images indicating that the densities of a BSFs and threading dislocations (TDs) for the nonpolar GaN layer grown on PSS were reduced to 5.47 × 10^5 cm^{-1} and 3 × 10^9 cm^{-2}, respectively, while the nonpolar GaN layer grown on planar substrate contained the high BSFs of 1.16 × 10^6 cm^{-1} and TD of 1.8 × 10^{10} cm^{-2}.[13] However, in the case of the semipolar GaN layers,[19] we could see that the FWHM values of on-axis (11$\bar{2}$2) XRCs for the semipolar GaN layer grown on PSS with different incident beam directions of [11$\bar{2}\bar{3}$] and [1$\bar{1}$00] seemed to be relatively broad compared to those of the nonpolar GaN layer grown on PSS. These values of the on-axis rocking curves for the semipolar GaN layers grown on planar substrate and PSS with an incident beam direction of [11$\bar{2}\bar{3}$] were 713 and 786 arcsec, respectively, whereas the FWHM values of both samples with an incident beam direction of [1$\bar{1}$00] were 1134 and 1080 arcsec, respectively. In regard to preceding reports, their associated PDs can broaden on-axis (11$\bar{2}$2) XRCs while none of the BSFs were visible under on-axis (11$\bar{2}$2) XRCs.[20] Therefore, these similar FWHM values of semipolar GaN layer grown on planar substrate and PSS suggested that both samples had similar density of PDs. On the other hand, for the off-axis (n0-n0) and (000n) XRCs FWHM values which were influenced by the BSFs and TDs respectively,[19] we could observed that the FWHM values of semipolar GaN layer grown on PSS were decreased compared with those of semipolar GaN grown on planar substrate (The reduction in BSFs was clearly shown in the cross-sectional TEM image in Fig. 3(b)). These indicated that the BSFs and TDs densities in the semipolar GaN were reduced by introducing the PSS technique.

Figure 4 exhibits the PL spectra of samples N1, N2, S1, and S2 at room temperature (detailed characteristics of these spectra are tabulated in Table 1). In this figure, it is seen that the emission intensity of sample N2 was about 3 times higher than that of sample N1, and the emission intensity of sample S2 was approximately 4.5 times higher than that of sample S1. Moreover, full width at half maximum (FWHM) values for samples N2 and S2 were also decreased by introducing the PSS technique. These enhanced optical properties of samples N2 and S2 were attributed to a reduction in defect density by the PSS patterns. On the other hand, a point worth noting in this figure was the results of the

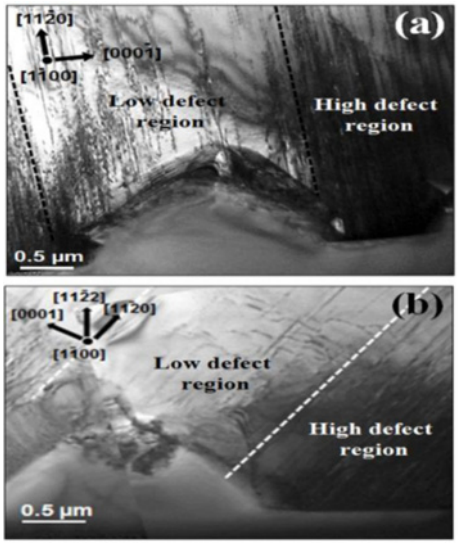

Fig. 3. Cross-sectional TEM images of samples (a) N2 and (b) S2 (Z = [1$\bar{1}$00], g = [11$\bar{2}$0]).

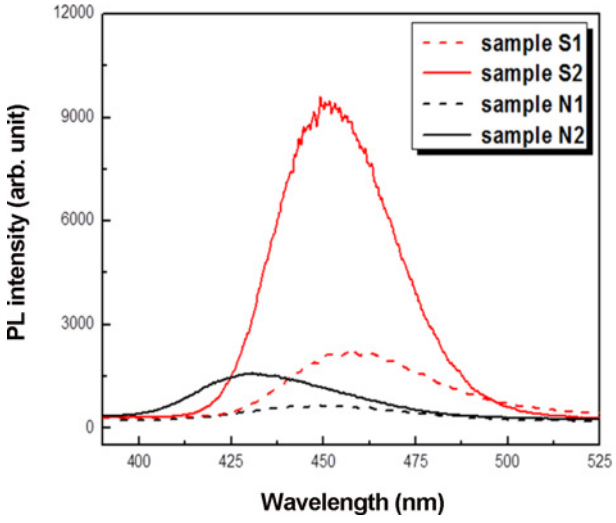

Fig. 4. Room temperature PL spectra of samples N1, N2, S1, and S2, respectively.

Table 1. Characteristics of PL spectra of samples N1, N2, S1 and S2.

	Nonpolar		Semipolar	
	N1	N2	S1	S2
Wavelength (nm)	449	431	457	449
Intensity (a.u)	470	1580	2020	9370
FWHM (nm)	50	46	42	36

semipolar samples in relation to those of the nonpolar samples.

In terms of optical quality, not only did sample S2 show the best optical performance, sample S1 also indicated better optical performance than sample N2, despite the use of a planar substrate for S1. Although its reason is unclear and will be studied further, one of the possible reasons is probably due to lower defect density of semipolar layer in comparison with nonpolar layer. In our previous study (not shown here),[21] we could confirm that BSFs density of semipolar GaN grown on planar sapphire substrate were 8.4×10^5 cm^{-1} which is considerably similar to that of nonpolar GaN grown on PSS (as mentioned above). From this result, it is supposed that sample S2 has the lowest defect density among all the samples. Furthermore, the emission wavelengths of samples N1 and S1 were 449 nm and 457 nm, respectively, and those of samples N2 and S2 were 431 nm and 449 nm, respectively. Although all the samples were grown under the same growth temperature, the semipolar samples showed wavelengths that were approximately 20 nm longer in comparison with the nonpolar samples. According to the report by Northrup *et al.*, the reason why semipolar $(11\bar{2}2)$ plane indicate higher indium incorporation is to have binding sites that may accommodate indium atoms more easily than either *c*- or *m*-plane.[22] In addition, Wernicke *et al.*[23] and Zhao *et al.*[24] also reported that the semipolar $(11\bar{2}2)$ plane has the highest indium incorporation rate among various planes. Therefore, all these results suggest that it is more beneficial to use semipolar $(11\bar{2}2)$ plane in In-rich InGaN growth.

To further understand the optical properties for semipolar QWs, μ-PL mapping measurements were additionally carried out on the semipolar samples. Figure 5(a) illustrates the μ-PL mapping images of the PL wavelength, intensity, and FWHM for sample S1. By comparing these three images, we found that some particular features were located in the same position [indicated as solid-line triangles in Fig. 5(a)]. The features were indicated as dark regions in the PL intensity image and as bright regions in the PL wavelength and FWHM images. Because the number and shape of these features were significantly akin to those of the arrowhead-like features shown in the previous OM image [see Fig. 2(c)], we could regard these features as the arrowhead-like features. This trend is more clearly seen in the inset figure of the intensity image, indicating the monochromatic CL image of sample S1 at 450 nm. In this connection, it was suggested that the arrowhead-like features may lead to an increase in the incorporation of In and act as nonradiative recombination centres, in that the features had long wavelengths with weak intensity and high FWHM value. In fact, it is unclear which aspects of the arrow-head-like features are accurately associated with the optical behaviour. A possible reason may be the high density of threading α-type dislocations or grain boundaries connected with some arrowhead-like features.[25,26] Taken under the same measurement conditions, the μ-PL mapping images of the PL wavelength, intensity, and FWHM for sample S2 are shown in Fig. 5(b). From the previous μ-PL mapping images, we could confirm that the surface morphological features, which are arrowhead-like features, had a strong influence on the optical properties of the luminescence. This characteristic is also exhibited in the μ-PL mapping images of sample S2. However, unlike sample S1, sample S2 showed not only arrowhead-like features (indicated as solid lines), but also spotty features (indicated as dashed circles), especially in the intensity mapping image. These spotty features were believed to be connected with the low-defect regions because the number, shape, and arrangement of the spotty features were quite similar to those of the PSS.

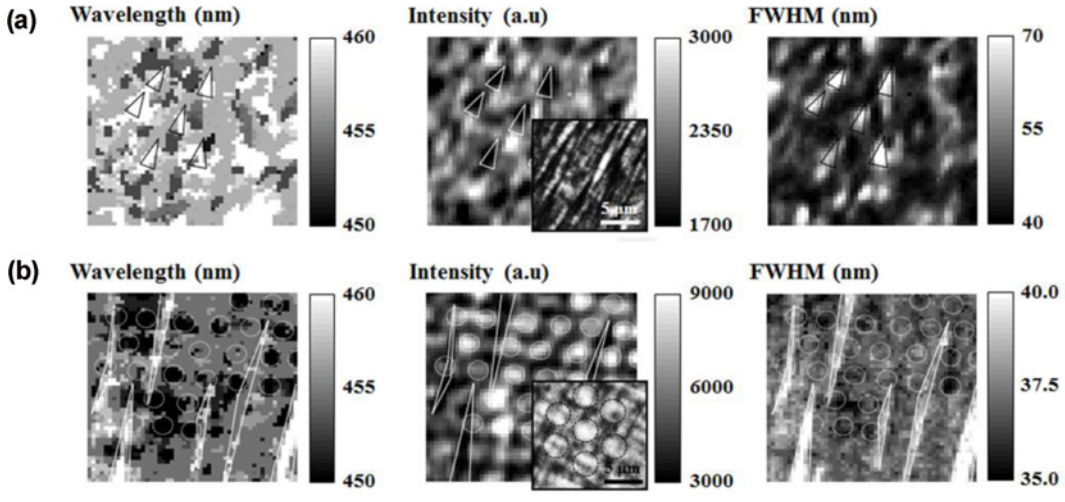

Fig. 5. (a) Micro-PL mapping images (25×25 μm^2) of the PL wavelength, intensity, and FWHM for (a) samples S1 and (b) S2. Inset figures indicated monochromatic CL images of sample S1and S2 at 450 nm.

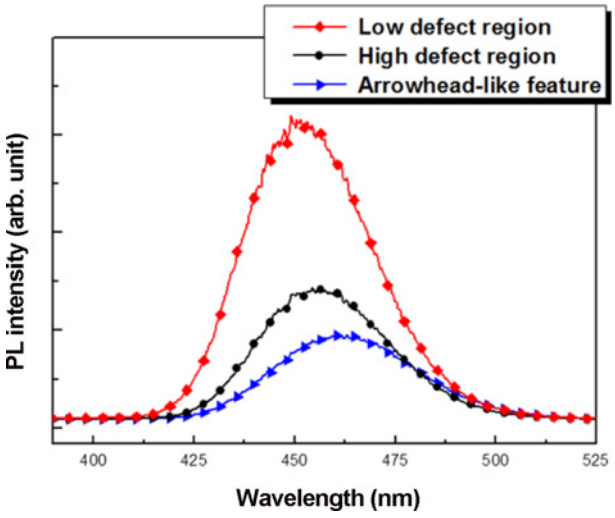

Fig. 6. Micro-PL spectra at different regions for sample S2.

Table 2. Characteristics of PL spectra of sample S2.

	Sample S2		
	Low-defect region	High-defect region	Arrowhead-like features
Wavelength (nm)	449	454	461
Intensity (a.u)	9370	4070	2640
FWHM (nm)	36	37	41

This argument is also supported by the fact that low-defect regions were formed by PSS patterns, which was seen in the TEM analysis. Thus, this observation implies that defect density and distribution had an influence on the optical properties of semipolar QWs as well.

To further investigate the luminescence properties in different regions of sample S2, μ-PL spectra were plotted in Fig. 6. As expected, arrowhead-like features showed the longest wavelength with the lowest intensity [see Fig. 5(a)], and QW emissions in the low-defect region showed higher intensity in comparison with those in the high-defect region (detailed characteristics of these spectra have been tabulated in Table 2). The interesting point is that these low- and high-defect regions had different peak wavelengths, as can be seen in Fig. 6. The emission peak wavelengths of the low- and high-defect regions were 449 and 454 nm, respectively, which implies that In incorporation is increased with high-defect density.

4. CONCLUSIONS

The characteristics of nonpolar and semipolar InGaN/GaN quantum wells grown on planar and patterned sapphire substrates were studied by structural and optical analyses. We observed that the number and size of the surface morphological features such as undulation and arrowhead-like features shown in the nonpolar and semipolar films, respectively, changed with the substrates. Moreover, for the nonpolar and semipolar QWs grown on PSSs, low-defect regions were formed by periodically aligned patterns that reduced the defect density, as verified by the cross-sectional TEM. PL measurements also revealed that semipolar $(11\bar{2}2)$ orientation is more promising for high In-containing InGaN growth, in that the semipolar QWs showed longer emission wavelengths and enhanced optical performance than do nonpolar $(11\bar{2}0)$ QWs. Especially for the semipolar samples, we confirmed that the luminescence of the semipolar films was affected by the typical surface morphology of the films, so that the samples had nonuniform optical properties. Furthermore, high defect density in the semipolar samples led to high In incorporation and low emission intensity.

ACKNOWLEDGEMENTS

This work was supported by Indus-trial Strategic Technology Development Program No. 10041188 and the National Research Foundation of Korea (NRF) grant funded by the Korea government (MEST) No. 2012R1A2A2A01011702.

REFERENCES

1. E. F. Schubert and J. K. Kim, *Science* **308**, 1274 (2005).
2. J. Wu, W. Walukiewicz, K. M. Yu, W. Shan, J. W. Ager, E. E. Haller, H. Lu, W. J. Schaff, W. K. Metzger, and S. Kurtz, *J. Appl. Phys*. **94**, 6477 (2003).
3. P. Kung and M. Razeghi, *Opto-Electron. Rev.* **8**, 201 (2000).
4. S. Nakamura and G. Fasol, *The Blue Laser Diode,* p. 201-60, Springer, Berlin (1997).
5. J. Wu, W. Walukiewicz, K. M. Yu, J. W. Ager, E. E. Haller, H. Lu, and W. J. Schaff, *Appl. Phys. Lett.* **80**, 4741 (2002).
6. P. Waltereit, O. Brandt, A. Trampert, H. T. Grahn, J. Menniger, M. Ramsteiner, M. Reiche, and K. H. Ploog, *Nature* **406**, 865 (2000).
7. F. Bernardini and V. Fiorentini, *Phys. Status Solidi B* **216**, 391 (1999).
8. M. C. Schmidt, K. C. Kim, H. Sato, N. Fellows, H. Masui, S. Nakamura, S. P. DenBaars, and J. S. Speck, *Jpn. J. Appl. Phys. Part 2* **46**, L126 (2007).
9. D. N. Zakharov, Z. Liliental-Weber, B. Wagner, Z. J. Reitmeier, E. A. Preble, and R. F. Davis, *Phys. Rev. B* **71**, 235334 (2005).
10. P. Vennéguès, Z. Bougrioua, and T. Guehne, *Jpn. J. Appl. Phys., Part 1* **46**, 4089 (2007).
11. P. D. Mierry, T. Guehne, M. Nemoz, S. Chenot, E. Beraudo, and G. Nataf, *Jpn. J. Appl. Phys., Part 2* **48**, 031002 (2009).
12. G. Yoo, H. Park, H. Lim, S. Lee, O. Nam, Y. Moon, C. Lim, B. Kong, and H. Cho, *Jpn. J. Appl. Phys.* **50**, 042103

(2011).
13. G. Yoo, H. Park, D. Lee, H. Lim, S. Lee, B. Kong, H. Cho, H. Park, H. Lee, and O. Nam, *Curr. Appl. Phys.* **11**, S90 (2011).
14. T. Gühne, Z. Bougrioua, P. Vennéguès, M. Leroux, and M. Albrecht, *J. Appl. Phys.* **101**, 113101 (2007).
15. D.-H. Lee, H.-J. Jang, B.-H. Kong, H.-K. Cho, and O. Nam, *Jpn. J. Appl. Phys.* **49**, 058001 (2010).
16. Y. Lee, T. Seo, A. Park, K. Lee, S. Chung, and E. Suh, *Electron. Mater. Lett*. **8**, 335 (2012).
17. Y. S. Lee, H. Kim, T. H. Seo, A. H. Park, S. B. Lee, S. J. Chung, C.-J. Choi, and E.-K. Suh, *Electron. Mater. Lett.* **9**, 587 (2013).
18. M. J. Kappers, J. L. Hollander, C. McAleese, C. F. Johnston, R. F. Broom, J. S. Barnard, M. E. Vickers, and C. J. Humphreys, *J. Cryst. Growth* **300**, 155 (2007).
19. J. Jang, K. Lee, J. Hwang, J. Jung, S. Lee, K. Lee, B. Kong, H. Cho, and O. Nam, *J. Cryst. Growth* **361**, 166 (2012).
20. M. A. Moram, C. F. Johnston, J. L. Hollander, M. J. Kappers, and C. J. Humphreys, *J. Appl. Phys*. **105**, 113501 (2009).
21. J. Jang, K. Lee, J. Hwang, S. Lee, K. Lee, and O. Nam, *9th International Conference on Nitride Semiconductors*, Glasgow, UK (2011).
22. J. E. Northrup, *Appl. Phys. Lett*. **95**, 133107 (2009).
23. T. Wernicke, L. Schade, C. Netzel, J. Rass, V. Hoffmann, S. Ploch, A. Knauer, M. Weyers, U. Schwarz, and M. Kneissl, *Semicond. Sci. Technol.* **27**, 024014 (2012).
24. Y. Zhao, Q. Yan, C. Y. Huang, S. C. Huang, P. S. Hsu, S. Tanaka, C. C. Pan, Y. Kawaguchi, K. Fujito, C. G. Van-de-Walle, J. S. Speck, S. P. DenBaars, S. Nakamura, and D. Feezell, *Appl. Phys. Lett*. **100**, 201108 (2012).
25. N. P. Hylton, P. Dawson, C. F. Johnston, M. J. Kappers, J. L. Hollander, C. McAleese, and C. J. Humphreys, *Phys. Status Solidi C* **6**, S727 (2009).
26. S. Y. Bae, D. S. Lee, B. H. Kong, H. K. Cho, J. F. Kaeding, S. Nakamura, S. P. DenBaare, and J. S. Speck, *Curr. Appl. Phys.* **11**, 954 (2011).